Fusion Engineering and Design 206 (2024) 114577

Contents lists available at ScienceDirect

Fusion Engineering and Design

journal homepage: www.elsevier.com/locate/fusengdes

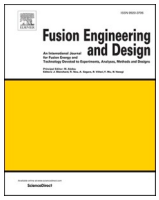

Manufacturing trials of PFCs with low thermal conductivity features for limiters

James Roberts [a,*], Ross MacDonald [a], Alex Russell [b], James Redman [b], Paul Brooker [b], Ian Bunce [c], Ethan Flynn [a]

[a] UK Atomic Energy Authority, Abingdon, United Kingdom
[b] TWI Ltd, Cambridge, Great Abington, United Kingdom
[c] Frazer-Nash Consulting, Leatherhead, United Kingdom

ARTICLE INFO

Keywords:
Plasma-facing component
High heat flux
Limiter
Tungsten
Manufacturing
Testing
Electromagnetic simulation

ABSTRACT

In future demonstration fusion power plants, plasma facing components will face high steady state and ultra-high transient heat loads from the plasma. Introducing low thermal conductivity features to the component can reduce the peak temperatures seen by the coolant pipe during transient loads, but at the trade-off of a loss of steady-state performance. Producing low-conductivity tungsten by additive methods has been investigated elsewhere, so this trial investigates production through subtractive means i.e., conventional milling. This method preserves the original temperature limits and majority of the microstructure and is much higher Technology Readiness Level (TRL) so requires less development to reach series manufacture. In this trial, diamond drilling produced holes in monoblocks down to 0.6 mm and ligaments down to 0.7 mm, showing that this method is capable of producing small features in a controlled way. With the geometric design of lattice used in this trial, these samples achieved thermal conductivity reductions of 15% to 40%. One monoblock assembly was tested up to 1100 °C for 500 cycles in the Heating by Induction to Verify Extremes (HIVE) High Heat Flux test rig and showed no signs of ligament cracking or thermal degradation. Electromagnetic modelling has been validated against the experimental results, so future designs can be accurately modelled ahead of testing in HIVE.

1. Introduction

Plasma-Facing Components (PFCs) optimised for steady-state operations require high thermal conductivity in order to minimise thermal gradients and stresses for a given heat flux.

However, for components with significant transient heat flux requirements, such as Limiters, a low-conductivity component is desirable. Low thermal conductivity features increase the transit time for a conducting transient thermal wave, which reduces the peak temperatures seen 'downstream' of the feature and therefore reduces the peak temperature seen by the coolant pipe [1]. This is essential in Limiters, where Vertical Displacement Event (VDE) loads are expected to be as high as 300GW/m^2 for 1 to 5 ms [2]. These extreme loads have the potential to weaken or even melt the coolant pipe and cause a Loss of Coolant Accident (LOCA) [3,4].

The trade-off is that the increased thermal resistance lowers steady-state performance, so the performance must be balanced between the competing steady-state and transient requirements [5].

Dedicated low-conductivity features offer a compact alternative to deep monoblock designs, with comparable total thermal resistance and lower cracking risk. These features may also offer a mechanical strain relief and crack arresting capability [6,7]. These features have been explored by the STEP programme with a generic monoblock PFC design. This design does not reflect the current status of the STEP Limiters but allows comparison of the low-conductivity feature with other existing tests.

2. Manufacturing

2.1. Low-conductivity layer

A layer of effective low-thermal-conductivity tungsten can be produced by removal of material. The thermal conductivity of the material itself remains the same, but by removing material there is a reduced area for heat to flow through. The removal of mass reduces conductivity by two mechanisms: the reduction of area and by increasing the distance of

* Corresponding author.
E-mail address: james.roberts@ukaea.uk (J. Roberts).

https://doi.org/10.1016/j.fusengdes.2024.114577
Received 1 May 2024; Received in revised form 28 June 2024; Accepted 29 June 2024
Available online 11 July 2024

the thermal path [6]. This means that when the total sample cross-section is considered, the effective conductivity across that cross section is reduced.

Therefore, to achieve a low-conductivity tungsten layer, it is desirable to create tungsten with reduced mass. This can be done with additive or subtractive methods. Additive methods have shown issues with cracking [8] and geometric conformity for small ligaments [9]. Subtractive methods have the benefit of preserving the properties and microstructure of the original tungsten. The expected downside is that tungsten is brittle and generally understood to be difficult to machine. Wire electrical discharge machining (EDM) is used for most tungsten subtractive machining operations, however, conventional milling is faster and less expensive, so is more appropriate for parts with a high number of features. In this trial, diamond drilling was used. Machining can lead to locally high temperatures, which could lead to a region of recrystallised tungsten around the hole. This could be investigated in future work.

One method of producing a lattice is to drill two sets of orthogonal holes, producing a unit cell as shown in Fig. 1. This produces an anisotropic unit cell, with open side faces and closed top and bottom faces, and the ligaments having a square cross section. The cell is oriented such that the direction of the heat flux is aligned with the narrow ligaments. This method of lattice production was chosen as it can be produced with only two orientations of drilling.

The lattice properties can be varied by changing the hole size and spacing, which can produce different volume fractions and ligament sizes. In this trial, lattice geometries were produced with hole sizes of 0.6 mm, 1.5 mm, and 2.4 mm. A minimum ligament size of 0.7 mm was specified to reduce the risk of cracking during production and testing, but this minimum could be reduced with further trials. The initial samples were 12 mm high blocks, as shown in Fig. 2.

The initial batch of samples were sectioned and micrographically inspected, and they showed high geometric consistency and no evidence of ligament cracking. The section in Fig. 3 shows good agreement with the specification of 0.7 mm by 0.8 mm ligaments.

After the lattice layer samples were produced and agreed to be of sufficient quality to proceed, sixteen monoblocks were produced with the lattice layer drilled directly into them. Six were produced with 0.6 mm holes, five with 1.5 mm holes and five with 2.4 mm holes. The hole geometries were preserved from the initial blocks, so all samples had a hole layer height of 10 mm.

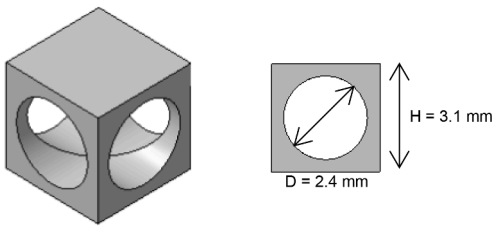

Fig. 1. Isometric and side view of the unit cell for the 2.4 mm lattice.

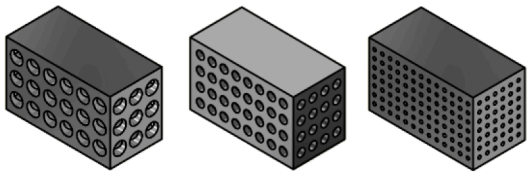

Fig. 2. Isometric view of the drilled lattice geometries for the 2.4 mm, 1.4 mm, and 0.6 mm hole layers. The outer dimensions of each sample are 20 mm by 12 mm by 10 mm.

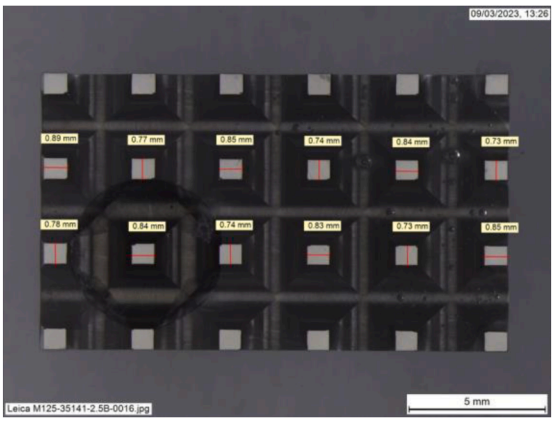

Fig. 3. A micrographic view of the 2.4 mm hole sample, sectioned through the narrowest extent of the ligaments. The pale rectangles are the ligaments and the darker regions between represent the holes.

2.2. Assembly joining

One substantial advantage of machining the layer directly into the tungsten monoblock is that no additional joins are required to include the low conductivity layer. This preserves the high temperature limits of conventional tungsten, which is essential for any PFC application, particularly one with ultra-high transient load requirements such as the Limiter. Any braze material or diffusion bond interlayer would introduce a locally lower temperature limit, so a design with a join between the low-conductivity layer and the armour above would not be possible due to the high temperatures in that region. Machining the holes means that no join is required above the layer.

Below the low-conductivity layer the operating temperature is much reduced, so a join is possible. Therefore, this design feature can work with either a tile-on-heatsink or monoblock style design. In either case, once the holes have been machined the armour component can be treated the same as any other tungsten armour component with a bulk interface, meaning that previous joining expertise with tungsten is applicable and a variety of techniques could be used.

For the sake of these test assemblies, a monoblock geometry was used, with a CuCrZr coolant pipe and a copper interlayer. The joining technique used was hot radial pressing [10], with the radial pressure introduced by differential thermal expansion. The monoblock design was chosen to provide a reliable test of the low-conductivity layer and provide input information into future down-selection of low-conductivity features.

The copper ring was cooled in liquid nitrogen whilst the tungsten block was heated in a furnace. The ring was then placed into the monoblock, creating an interference fit at room temperature. This was done for four monoblocks, then the pipe was cooled in liquid nitrogen and placed inside the room-temperature monoblock and ring assemblies, using an alignment jig. This created an interference fit between the three sets of components, generating the radial force for the diffusion bond. This thermal expansion method allowed for the fast production of a small number of samples, without the dedicated pipe pressurisation

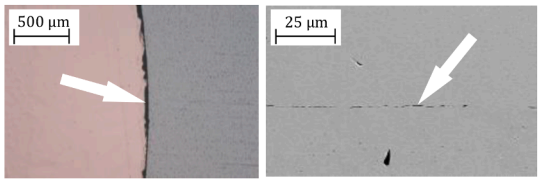

Fig. 4. A micrographic view of the Cu/W interface (left) and an SEM view of the CuCrZr/Cu interface (right) of the sectioned 825 °C diffusion bond sample. Voids are indicated by the white arrows.

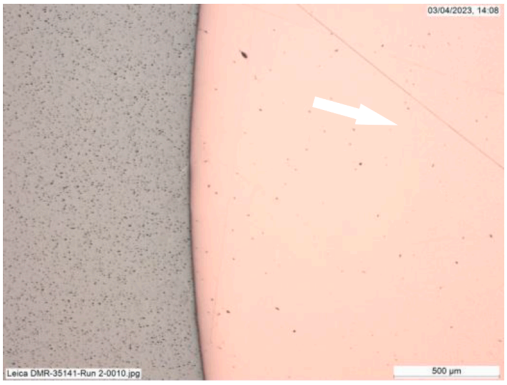

Fig. 5. A micrographic view of the sectioned diffusion bonding test run 2 sample. The CuCrZr/Cu bond region is indicated by the white arrow.

equipment described in [3].

The assembly was then placed in a vacuum furnace and held at temperature for 4 h, creating diffusion bonds at the CuCrZr/Cu and the Cu/W interfaces. Trials were performed at 825 °C and 1000 °C, with the expectation that 825 °C runs would better preserve the precipitate hardening of the CuCrZr pipe and the 1000 °C runs would produce the best bond quality. Fig. 4 shows the results of the 825 °C run, showing voids at the Cu/W interface in the micrograph and a lack of diffusion at the CuCrZr/Cu interface in the SEM image.

Fig. 5 shows the results of the 1000 °C run, showing a lack of voids at the W/Cu interface and an invisible bond line at the CuCrZr/Cu interface, indicating that diffusion has occurred at both interfaces.

Fig. 6 shows an SEM view of the tungsten-copper interface for a 1000 °C run. The expected diffusion layer depth is in the nanometre range [11], so no visible diffusion can be seen. However, it is noted that there are no observable voids or inclusions, indicating a satisfactory bond.

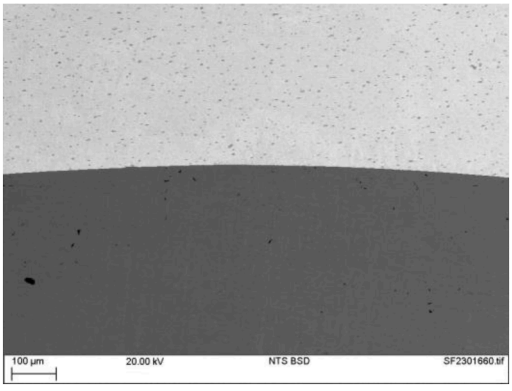

Fig. 6. An SEM view of the sectioned diffusion bonding test run 2 sample.

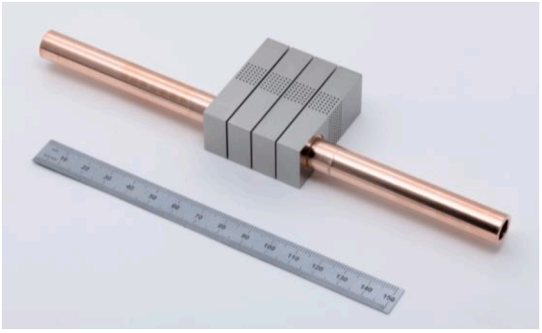

Fig. 7. The 0.6 mm monoblock sample after final sample assembly.

Part of the same sample was sectioned along the pipe length and subject to radial impacts. The join remained intact whilst the pipe yielded and the tungsten fragmented, further indicating sufficient join quality for the purposes of this trial.

Holding the assembly at 1000 °C will have degraded the properties of the CuCrZr pipe. However, as the assembly joining was not the focus of this trial, it was decided not to optimise the bonding parameters further and to use the 1000 °C parameters for the final assemblies.

Four assemblies of four monoblocks onto a CuCrZr pipe were produced: one with 0.6 mm holes, one with 1.5 mm holes, one with 2.4 mm holes, and one with a mix of all three hole sizes. The 0.6 mm hole assembly is shown in Fig. 7.

3. Testing

3.1. Experimental set-up and methodology

The 0.6 mm and 2.4 mm hole assemblies were tested in HIVE (Heating by Induction to Verify Extremes) at UKAEA to assess their thermal performance and test the cyclic performance of the ligaments.

In HIVE a 45 kW, 50–150 kHz industry standard induction heating system is used as the power source. An induction coil couples to the sample and induces volumetric currents, leading to Ohmic heating of the sample. High frequency power leads to shallow 'skin depth' and therefore quasi-surface heat loads. Achievable average heat fluxes of up to 15 MW/m^2 equivalent, dependent on part size and coil geometry.

HIVE can run samples either uncooled or water cooled. It has a closed loop pressurised cooling system capable of a maximum temperature of 200 °C and a maximum pressure of 20 bar, and a High Vacuum system capable of vacuum pressures down to 1×10^{-7} mbar. For these tests, the coolant inlet conditions were 25 °C and ~1 bar, at a flowrate of 17.5 L/min. These parameters were chosen to maximise the thermal gradient across the lattice, rather than to maximise the possible heat flux, which

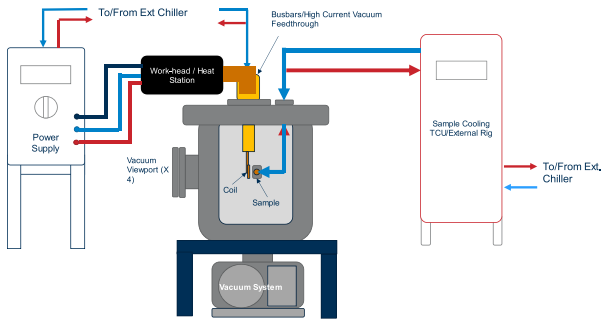

Fig. 8. A profile schematic of the HIVE Facility, including a cross-section of the vacuum vessel.

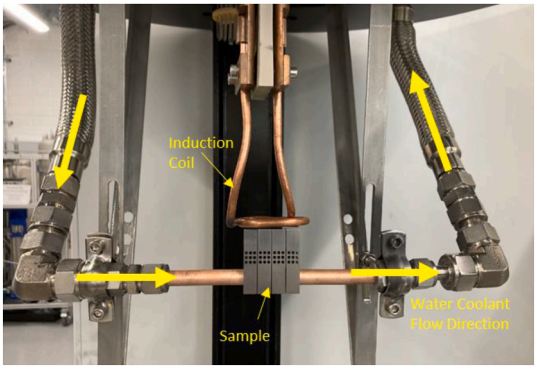

Fig. 9. The 2.4 mm hole sample fitted to the HIVE lid, with cooling connections and induction coil fitted.

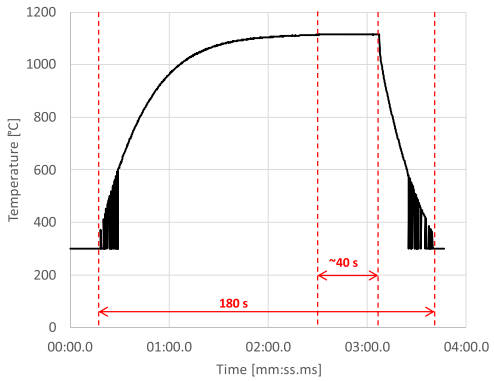

Fig. 10. Trace of pyrometer reading for a representative cyclic loading test pulse (pulse 266), showing the 180 s duration of the heating and the ~40 s steady-state period.

would be achieved at higher coolant flow rate and pressure. The thermal gradient defines the induced strain, and as the focus of the trial is cracking of the ligaments, the induced strain is the key parameter to control for this trial.

All sample instrumentation was mounted on the four equatorial vacuum viewports labelled in Fig. 8. The instrumentation used on this test was:

- FLIR SC7500 Medium Wave IR camera
- Sensotherm M322 2-spot pyrometer
- Olympus OM-1 digital camera

Thermocouples provide inlet and outlet coolant information, which can be used to evaluate the thermal power deposited into the sample. This can be used to give heat flux delivered to the sample, using temperature-based adjustments if heating is uneven. The cooling arrangement and sample mounting is shown in Fig. 9.

The 0.6 mm sample was tested with a single-run performance test. The 2.4 mm sample underwent 500 cycles of heating. The 1.5 mm sample and the mixed-type sample were not tested.

During experiment commissioning, the coolant conditions were set, and the heat flux increased to reach the desired temperature values. A total pulse duration of 180 s was chosen, as this gave time for all thermocouple readings to stop increasing and gave a dwell time at steady-state of ~400 s, as shown in Fig. 10.

Test parameters were set by front face temperature rather than heat flux, with a limit of 1200 °C based on recrystallisation [3]. The orientation of the sample meant that the pyrometer had to read the side face rather than the front face, so the pyrometer limit temperature was set as 1100 °C.

For the 0.6 mm and 2.4 mm samples with these cooling parameters, the required heat flux in HIVE was 4.4 and 2.2 MW/m^2 to reach the target temperatures respectively. For the same temperature limits and hole geometry, higher heat fluxes would be possible with shorter bulk tungsten armour or a higher coolant flow rate and pressure.

3.2. Description of results

With the coil geometry used, both samples showed strong heating of the centre two monoblocks, as can clearly be seen from the visible radiation in Fig. 11. The peak IR temperatures recorded for the 2.4 mm sample across the four blocks were: 852 °C, 1188 °C, 1175 °C and 729 °C. With further electromagnetic modelling based on the work in Section 4, a coil geometry could be optimised to heat the four blocks more evenly.

As emissivity of the surface strongly affects the temperatures read by the IR camera, the sample was sprayed with graphite spray to fix its emissivity to a known value of 0.9. The grey spray can be seen in Fig. 11. As can be seen in Fig. 12, the IR results show that the temperature is much higher above the hole layer, then drops rapidly through it.

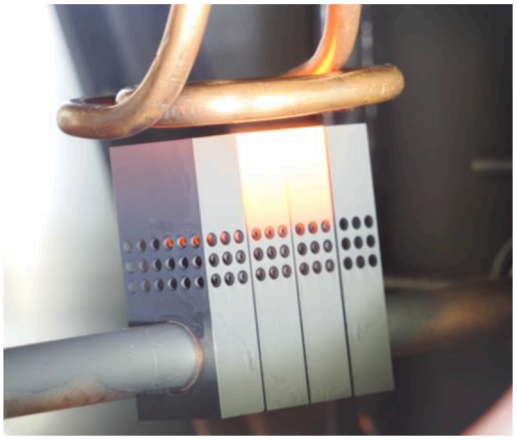

Fig. 11. Photograph of the 2.4 mm sample on test.

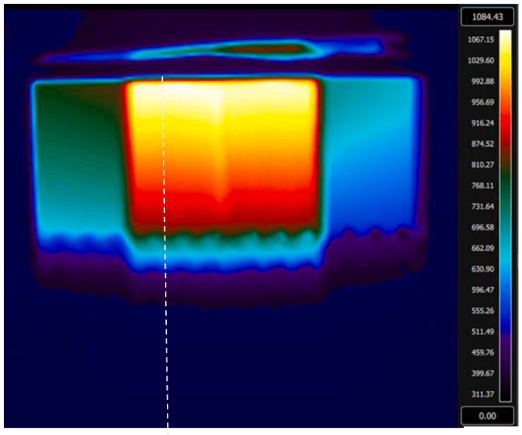

Fig. 12. Infrared capture of the 2.4 mm sample during testing. The line along the face of the second monoblock is used to produce the temperature plot in Fig. 13.

A linear plot of the IR data shows the change in effective conductivity clearly, with Fig. 13 showing an increase in gradient through the hole layers.

For the 500-count cyclic testing, the 2.4 mm hole sample assembly was removed after every 125 cycles and visually inspected for any

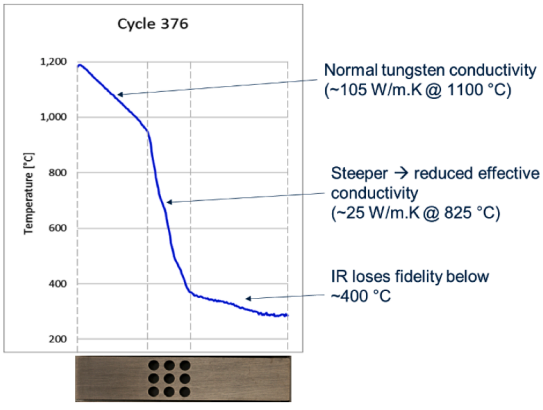

Fig. 13. Linear plot of the temperature against length through the 2.4 mm sample.

Table 1
Thermal performance of monoblock samples.

Hole Size (mm)	Volume reduction	Reduction in effective thermal conductivity
0.6	17%	15%
2.4	47%	40%

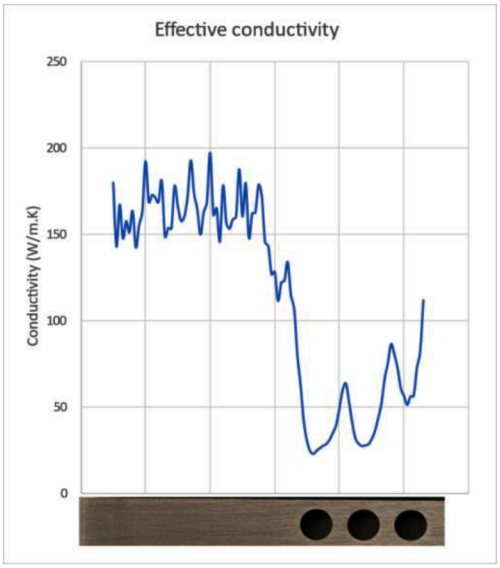

Fig. 14. Plot of effective conductivity through sample position, for the 2.4 mm sample.

damage to the ligaments, and the graphite spray reapplied. No damage was observed at any interval. If multiple ligaments cracked during testing, this would be reflected in an increase in temperature of the block above the hole layer, as seen in previous tests on lattice structures [12]. Throughout the experiment the measured temperatures remained similar, indicating the absence of severe failures in the lattice.

The 0.6 mm sample and 2.4 mm sample showed different reductions in conductivity, as shown in Table 1. The results indicate that the reduction in effective conductivity is closely related to volume reduction.

From the temperature results, local thermal conductivity can be calculated, as shown in Fig. 14. In this calculation, the noise from the IR reading is amplified, but the reduction in thermal conductivity through the hole layer can clearly be seen. At the lower end of the layer, the tungsten is cooler, so the effective conductivity increases as the underlying thermal conductivity of the tungsten increases significantly at these temperatures [13].

4. Electromagnetic modelling

The capability to simulate the coupled electromagnetic and thermal behaviour of a Monoblock, or other PFCs, is useful for optimizing both the design of components and HIVE induction coils. A model of the 2.4 mm hole Monoblock was created in Altair Flux 2022.2 software to compare simulated results with the surface temperatures and power dissipated into the coolant measured during testing on HIVE.

4.1. Analytical set-up and methodology

The electromagnetic formulation used in this analysis becomes unreliable when the geometry allows for current loops, so including the hole layer in the electromagnetic model would have increased the computational complexity. The lower section of a monoblock sees only a small amount of induced heating, as the skin effect results in the current being concentrated in the top face. On this basis, the lower sections of the monoblocks were excluded from the electromagnetic calculation with the split line crossing through the top layer of holes as shown in Fig. 15. The entire assembly is included in the thermal model.

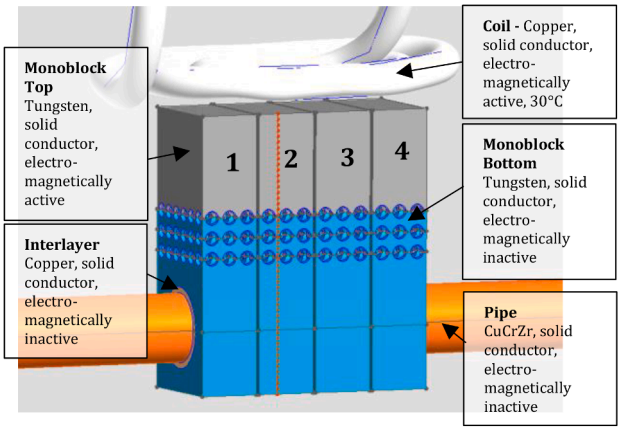

Fig. 15. Screenshot of the monoblock geometry in Flux. The different volume regions and their corresponding settings are labelled. The dashed-red line along the face of monoblock 2 is used to produce the temperature plot in Fig. 17.

Tungsten, CuCrZr and copper materials were modelled using temperature-dependent material properties and applied to the simulation geometry as shown in Fig. 15. The coil and its placement relative to the sample was modelled by referencing orthographic photos of the coil and sample set up in HIVE. The coil has its temperature controlled at 30 °C using a boundary condition, as it is water cooled.

The monoblock was meshed using 0.1 mm elements from the front face to the skin depth of ~0.34 mm, to ensure a minimum of two elements are used in the skin depth. The remaining geometry was meshed automatically using the default settings.

All external faces of the geometry had radiation to infinity applied. The front and camera-side faces had a graphite coating applied, so they are modelled with an emissivity coefficient of 0.9. The remaining faces have an emissivity of 0.25 to approximate tungsten. The faces between the monoblock segments and inside the limiter holes did not have radiation applied, as simulating local radiation significantly increases solving complexity. The inside surface of the coolant pipe has convective heat transfer with an HTC driven by the local temperature. The temperature vs HTC curve was calculated using the HIVE parameters described in Section 3.1.

The coupled magnetic & thermal model was solved until the steady-state thermal condition was reached, with the current through the coil set at 480 A and 101 kHz.

4.2. Description of results

The simulation results were broadly representative of the temperature and power measurements taken during the real HIVE test. The induced heating power in the monoblock was 945 W, the power lost via radiation was 73 W and the power lost via the water cooling was 872 W. This is close to the measured water-cooling power of 868 W. These values also suggest that the steady-state thermal condition was reached, as all power flows in and out of the monoblock are accounted for:

$$945 + (-73) + (-872) = 0 \text{ W}$$

The peak front face temperature of the monoblock was 1063 °C, which is slightly less that the measured peak of 1100 °C. This could be due to variations in emissivity, which both the pyrometer and the modelling are sensitive to. It could also be due to inaccuracy in the coil modelling and position inducing a different current pattern without such a concentrated peak. Segments 2 & 3 have higher temperatures than 1 &

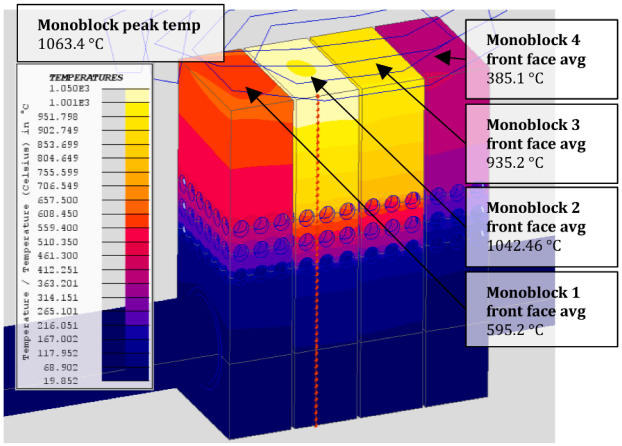

Fig. 16. Monoblock surface temperature distribution at steady-state. The Average front face temperatures and overall peak temperature are labelled.

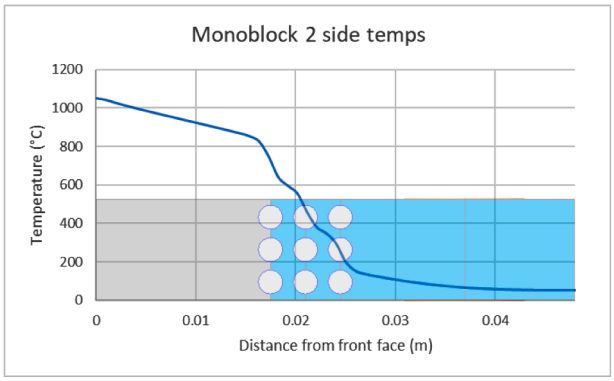

Fig. 17. Surface temperature through depth of monoblock 2 (see Fig. 13), from the front face (0 m) to back face (0.048 m).

4 (as shown in Fig. 16), which was also observed in reality and is a result of the coil design and corresponding heat distribution.

The low-conductivity layer shows the expected drop in thermal conductivity, resulting in a significant temperature decrease after each layer of holes. This can be seen graphically in Fig. 16 and is also plotted in Fig. 17, which shows a temperature distribution similar to the experimental data plotted earlier in Fig. 13. Monoblocks 1 & 4 show lower temperatures than the IR plot, which could again be due to the lack of local radiation modelling creating a larger temperature differential between the central and outer monoblocks.

Overall, the simulated results align reasonably well with the experimentally measured results, with scope to be developed further for digital testing of future PFC designs prior to physical testing. Although discrepancies remain between the simulated and experimental results, these may be attributed to the lack of local radiation modelling, or to small inaccuracies in the modelled coil geometry and placement. Future simulation work will aim to improve accuracy by addressing these issues.

5. Conclusions

The results show that machining holes into tungsten is an effective way of reducing the thermal conductivity of the tungsten based PFCs, which is crucial for the design of a Limiter which can withstand ultra-high transient heat loads [2–4].

The manufacturing results showed consistent geometric alignment and no micrographic evidence of cracks, whilst producing hole sizes down to 0.6 mm and ligament sizes down to 0.7 mm. The thermal testing also showed a significant reduction in the effective thermal conductivity in the layer, and a good controllability of the conductivity by varying the volume reduction, with reductions of between 15% and 40% achieved. The cyclic High Heat Flux testing showed no evidence of crack initiation or propagation after 500 cycles.

The flexibility of the approach offers significant design space, particularly in the arrangement and patterning of holes to control heat flow, or in the machining of larger openings. Further work could also investigate the mechanical compliance of the lattice structure, and the possibility for the holes to arrest cracks.

The trials have shown that machining of holes is a high-TRL alternative to additive manufacture methods to produce lattice-like PFCs, with comparable performance under steady state cyclic loading. A key piece of future work will be the analysis and testing against high energy transients, which is essential to evaluate the layer's primary protective function.

CRediT authorship contribution statement

James Roberts: Writing – original draft, Methodology, Conceptualization. **Ross MacDonald:** Writing – original draft, Methodology, Investigation. **Alex Russell:** Resources, Methodology, Investigation. **James Redman:** Resources, Methodology, Investigation. **Paul Brooker:** Resources, Methodology, Investigation. **Ian Bunce:** Supervision. **Ethan Flynn:** Writing – review & editing, Supervision.

Declaration of competing interest

The authors declare that they have no known competing financial interests or personal relationships that could have appeared to influence the work reported in this paper.

Data availability

Data will be made available on request.

Acknowledgments

This work has been funded by STEP, a UKAEA programme to design and build a prototype fusion energy plant and a path to commercial fusion.

The authors want to thank the HIVE team at UKAEA for their support during testing and subsequent analysis, and Terry O'Sullivan for his support during the manufacturing trials.

References

[1] R. De Luca, et al., Pre-conceptual design of a PFC equipped with a W lattice armour for first wall limiters in the EU-DEMO fusion reactor, Fusion Eng. Des. 191 (2023) 113742.
[2] F. Maviglia, et al., Integrated design strategy for EU-DEMO first wall protection from plasma transients, Fusion Eng. Des. 177 (2022) 113067.
[3] J.H. You, Limiters for DEMO wall protection: initial design concepts & technology options, Fusion Eng. Des. 174 (2022) 112988.
[4] T.R. Barrett, Progress in the engineering design and assessment of the European DEMO first wall and divertor plasma facing components, Fusion Eng. Des. 109-111 (2016) 917–924.
[5] R. De Luca, et al., Comparison between finite element and experimental evidences of innovative W lattice materials for sacrificial limiter applications, Fusion Eng. Des. 169 (2021) 112493.
[6] R. De Luca, et al., Preliminary investigation on W foams as protection strategy for advanced FW PFCs, Fusion Eng. Des. 146 (2018) 1690–1693.
[7] R. De Luca, Parametric design study of a substrate material for a DEMO sacrificial limiter, Fusion Eng. Des. 158 (2019) 111721.

[8] D. Wang, et al., Cracking in laser additively manufactured W: initiation mechanism and a suppression approach by alloying, Mater. Des. 162 (2019) 384–393.
[9] N. Mantel, et al., Development and testing of an additively manufactured lattice for DEMO limiters, Nuclear Fusion 62 (2022) 036017.
[10] E. Visca, et al., Manufacturing and testing of ITER-like divertor plasma facing mock-ups for DEMO, Fusion Eng. Des. 136 (2018) 1593–1596.
[11] J. Zhang, et al., Direct diffusion bonding of immiscible tungsten and copper at temperature close to Copper's melting point, Mater. Des. 137 (2018) 473–480.
[12] J. Pearl, et al., Cyclic medium heat flux testing of a WTa lattice structure on the HIVE facility, Fusion Eng. Des. 194 (2023) 113699.
[13] M. Fukuda, et al., Thermal properties of pure tungsten and its alloys for fusion applications, Fusion Eng. Des. 132 (2018) 1–6.